Ni-Sinapic Acid Nanocomposite in the Selective Sensing of Permanganate ions

[1]Prasenjit Mondal, [2]Pritam Singh, [3]David Morgan, [1]Adity Bose[*], [2]Kamalika Sen[*]

[1]Department of Chemistry, Presidency University, 86/1 College Street, Kolkata 700073, India

[2]Department of Chemistry, University of Calcutta, 92, APC Road, Kolkata 700009, India

[3]Cardiff Catalysis Institute, School of Chemistry, Cardiff University, Park Place, Cardiff, CF10 3AT, U.K.

Email: adity.chem@presiuniv.ac.in, kamalchem.roy@gmail.com

Abstract: A polyphenolic acid assisted synthesis of Ni nano particles for absorption spectrophotometric sensing of MnO_4^- ions in micro molar range is reported here. The synthesis was carried out using a green approach where sinapic acid acts as a capping agent. The synthesized nano particle was then characterized using UV-Vis spectroscopy, Fourier transform infrared spectroscopy, transmission electron microscopy, powder X-ray diffraction analysis, X-ray photoelectron spectroscopy. The particle size is around 5 to 10 nm with the presence of both porosity and nano crystallinity as obtained from the transmission electron microscopic analysis. This nano particle can selectively sense permanganate ions in presence of different co-existing ions with the limit of detection 0.413 µM. The sensing mechanism was examined with the isothermal titration calorimetry (ITC) and X-ray photoelectron spectroscopy (XPS). Isothermal titration calorimetric data suggests that the interaction between permanganate and the nano particle is enthalpy driven process with ΔH and ΔG values are -80 kcal/mol and -5.72 kcal/mol respectively. XPS data confirmed the presence of Ni(II) ions in the Ni-SA NPs and the atomic percentage of the same differed in presence of $KMnO_4$. There was no significant interference from the contemporary ions and even in the presence of Mn^{2+} ion. The method has also been applied for the natural water samples and for vegetable. ~88 to 108 % of the added $KMnO_4$ could be recovered from the tap water sample using our prepared methodology. The limit of detection and the present technique are compared with previously reported literature and have been found to be comparable, even in solvent-free conditions and using simple instrumentation.

Keywords: Sinapic acid; nickel sulphate; nano particle; sensing; potassium permanganate; limit of detection

1. Introduction

Nanotechnology has become one of vastly growing research fields in the modern science community. In recent years, metals like Fe, Co and Ni have received an immense interest as nanoparticles for their beneficial applications in different fields. Nano-structured materials have found applications in chemical sensing [1, 2], magnetic resonance imaging [3, 4], memory storage devices [5], catalysis [3, 6-8], drug delivery [9, 10], and very recently in the treatment of cancer cells [11]. One of such metal nanoparticles is Ni-based nanoparticles that can be a good semiconductor with their band gap energy in the range 3.6 to 4 eV [12].Additionally, Ni nanoparticles have a great potential for application in various pharmaceutical synthesis [13, 14], like magnetic biocatalysis [15], biomolecular separation [16], biosensor, [17] etc. They have different applications in several other fields [18], [19, 20], [21, 22], [23-25]. Various processes have been utilized to prepare the Ni nanoparticles of different shape and size, which include sol-gel method [26], electrodeposition [27], thermal decomposition of organic complexes [28], chemical reduction [29], co-precipitation [30], solvothermal methods [31, 32], etc. In order to avoid the tedious protocol and the sophisticated instrumentation associated with such methods, green synthesis can be a better option to reduce the use of toxic chemicals and make the process economically more viable [33, 34]. One such green methodology to synthesis metal-based nanoparticles is to use plant extract or naturally occurring substances that can act both as capping and reducing agents. Gebretinsae et al., reported the synthesis of nickel oxide nanoparticles using cactus plant extract [12]. Whereas, Karpagavinayagam et al., used *Avicennia Marine* leaf extract [35] for this purpose. NiO nanoparticles can also be synthesized using egg white [36].

Sinapic acid, a well-known phenolic acid is extensively found in nature, especially vegetables, fruits and a variety of beverages like tea, coffee, etc. It has various pharmacological potentials such as anti-inflammatory, anti-oxidant, anti-bacterial, anti-cancer, anti-anxiety, etc. [37-39]. Due to such activities, researchers have paid a great attention to utilise it in developing food, cosmetics and pharmaceutical products. In our recently published paper, we have already shown that sinapic acid also acts as a Cu(II) sensor with a detection limit of 64.5 nM [40]. Most of the researchers confirmed that the presence of phenolic acids in the plant materials are involved in the reduction and stabilization of metal ions [41].

One of the most important applications of permanganate is its use as an oxidizing agent as the central metal ion (Mn) is in the highest oxidation state [42]. The reduction potential of MnO_4^- /Mn^{2+} redox couple is 1.51 V in acidic solution. Besides, the permanganate ion is also used in disinfection of water [43], removal of pollutants like As(III) [44] and harmful organisms [45-47], treatment of skin infections like, acne, canker sores, fungal infections, etc., [43, 48]. Permanganate is used in water treatment plant [49], treatment of diseases in fish [50], washing of vegetables, as an effective sanitary reagent for the reduction of bacterial growth [51] and so on. On the other hand, Mn(II) is an essential trace element in human body governing the metabolic activity [52, 53], it can also be an important constituent for the accurate function of brain, nervous system, enzyme actions, lipid metabolism, growth of bone [54, 55], etc. Dysfunction of central nervous system, neurological disorder, hallucination, mental depression, harmful effects on respiratory, cardiac and reproductive system, problem with DNA mutation, are the most severe consequences of exposure to the excess concentration of Mn(VII) ions. It is therefore important to measure and control the amount of Mn(VII) entering into the body. Adulterated foods often contribute as a major source of Mn(VII) to the human body. At the same time drinking water treated with a requisite amount of Mn(VII), can also be considered as a potential source of this species. WHO has recommended a lower limit of Mn is 9.1 µM in the drinking water [56]. Therefore, it is essential to develop an appropriate method to detect Mn(VII) accurately and efficiently in food and water samples. Quite a few number of analytical methods like, spectrophotometry [52], inductively coupled plasma-optical emission spectrometry [52], inductively coupled plasma-mass spectrometry, atomic absorption spectroscopy [57], ion chromatography [57], etc., are reported in the literature for detection of Mn. But these methods either use toxic solvents or need high temperatures or complicated reagent synthesis or are not sensitive to the oxidation state. A detailed literature report describing the sensing of permanganate ion with their limit of detection and methodology is provided later in this article (Table S1).

Here we report an easy and economically favourable methodology for selective and sensitive detection of permanganate ions in water sample. First we have synthesized Ni- SANPs in water-ethanol mixed solvent. Then the synthesized nanocomposite was characterized using different analytical tools like, Fourier transform infrared spectroscopy (FTIR), transmission electron

microscopy (TEM), powder X-ray diffraction (PXRD) analysis, etc. It is important to understand the background of the interaction process between $KMnO_4$ and Ni-SA NPs in thermodynamics point of view. Isothermal Titration Calorimetric (ITC) titration was taken up as they provide direct values of ΔH, ΔS as well as stability constant and help to interpret forces of interaction involved [58, 59, 60]. The synthesized nanocomposite was then utilized towards spectrophotometric sensing of permanganate ion in water sample. The method was then further employed for the detection of permanganate ion in natural water samples and in vegetable.

2. Materials and Methods

2.1. Materials

Sinapic acid (SA) was purchased from Sigma Aldrich, USA. Nickel(II) sulfatehexahydrate ($NiSO_4.6H_2O$) (≥98 %) were purchased from Merck, India. Potassium permanganate ($KMnO_4$) (≥99 %), sodium arsenate dibasic heptahydrate ($Na_2HAsO_4.7H_2O$) (99-102 %), sodium chloride (NaCl) (≥99 %), sodium iodide (NaI) (≥99 %), sodium fluoride (NaF) (≥99 %), potassium dichromate ($K_2Cr_2O_7$) (≥99 %), sodium molybdate dehydrate ($Na_2MoO_4.2H_2O$) (≥99 %), sodium peroxidisulfate ($Na_2S_2O_8$) (≥99%), sodium selenate (Na_2SeO_4) (≥99 %), sodium selenite (Na_2SeO_3)(≥99 %), sodium sulfate (Na_2SO_4) (≥99 %), sodium sulfite (Na_2SO_3) (97-100 %), sodium thiosulfate ($Na_2S_2O_3$) (99-100 %) were purchased from Merck, India. Sodium arsenite (Na_3AsO_3) (≥98.5 %) was obtained from S.D. Fine Chem, India. All the required experimental solutions were prepared using triple distilled water. Boring water samples were collected from Garia, Dist.-South 24 parganas, West Bengal, India and from Sonarpur, Dist.- South 24 parganas, West Bengal, India. Tap water sample was collected from Rajabazar, Kolkata, West Bengal, India. Sweet potato was purchased from the local market. All other reagents were of analytical grade and used without further purification.

2.2. Apparatus

A powder X-ray diffractometer Rigaku Smart Lab Automatic High Resolution Multipurpose PC Controlled X-Ray Diffractometer System was used for the X-ray diffraction pattern of the nanoparticles. The analysis of functional groups was performed using a Perkin-Elmer L120-00A Fourier Transformed Infrared Spectrometer with sample as KBr pellets. The morphological features of the Ni based NPs was studied using transmission electron microscope (TEM) JEOL

JEM 2100 HR with EELS. The planes obtained from the selected area electron diffraction (SAED) pattern of the NP sample have been assigned with the help of imageJ software. UV-Vis spectroscopy was done using Agilent 8453 diode array spectrophotometer and Hitachi UV-Vis U-3501 Spectrophotometer. The change in thermodynamic parameters was examined using Malvern MICROCAL PEAQ-isothermal titration calorimetric (ITC) instrument. A Kratos Axis Ultra DLD system was used to collect X-ray photoelectron spectra (XPS) using monochromatic Al Kα X-ray source operating at 144 W (12 mA × 12 kV).

2.3. Synthesis of sinapic acid based Ni- nanoparticles (Ni-SA NPs)

A 10 mM SA solution was prepared in 1:4 ethanol-water mixture of pH~11. A10 mM $NiSO_4$ solution was also prepared in water. Equal amounts of these two solutions were then mixed and kept at 40 °C for 24 hours. The solution was evaporated using an IR-lamp. The residue was washed with 1:4 ethanol-water mixture and collected for further experiment.

3. Characterization

3.1. UV-Vis Spectroscopy

After the formation of the NPs, the characterization of the NPs was carried out using absorption spectroscopy. 5 mg of the solid NPs was taken in 0.5 mL of water and then sonnicated for 30 min. This NP solution was then analyzed using UV-Vis spectrophotometer and then compared with the spectra obtained for pure sinapic acid.

UV-Vis spectroscopy was further applied for the sensing study. 2 mL of water was taken in a quartz cuvette and treated with measured aliquots of the NP-solution. Different examined analytes of definite volume was then added to this solution and the results were analyzed using UV-Vis spectroscopy.

3.2. Fourier Transform Infrared Spectroscopy (FTIR)

The bond vibrations of the NPs were determined using FTIR analysis. Using a mortar-pestle, a small amount of the solid NPs was thoroughly mixed with dry KBr. The sample was then

pelletized using a hydraulic press at a pressure of around 5 ton. The pellet was then placed in the analyzer instrument's sample holder.

3.3. Transmission Electron Microscopy (TEM)

The sample for TEM analysis was obtained after dissolving 2 mg of Ni-SANPs in 2 mL of water-alcohol (1:1) combination and sonication for 1 hour. The dispersed solution was then dropped on a Cu grid with carbon coating. The grid was dried under an IR lamp prior to TEM imaging.

3.4. Powder X-ray Diffraction Analysis (PXRD)

The crystalline nature of the produced NPs was determined using powder XRD. Before the X-ray crystallographic study, the powder sample was placed on a rectangular glass holder and then introduced in front of the X-ray.

3.5. X-ray Photoelectron Spectroscopy (XPS)

XPS data was collected with pass energies of 160 eV for survey spectra, and 40 eV for the high-resolution scans with step sizes of 1 eV and 0.1 eV respectively. Samples were pressed into copper washers attached, using doubled sided Scotch tape (type 665), to a UV-Ozone cleaned glass microscope and pressed flat with a second clean glass slide.

The system was operated in the Hybrid mode, using a combination of magnetic immersion and electrostatic lenses and acquired over an area approximately 300 × 700 μm^2. A magnetically confined low energy electron charge compensation system was used to minimize charging of the sample surface, and all spectra were taken with a 90° take of angle. A base pressure of ~ 1×10^{-9} Torr was maintained during collection of the spectra.

Transmission corrected spectral data was analysed using CasaXPS (v2.3.25) [61] after subtraction of a Shirley background and using modified Wagner sensitivity factors as supplied by the manufacturer. Charge calibration was made to the lowest binding energy component from the fitted C(1s) spectra of each sample, the value of which was taken to be 285 eV.

3.6. Sensing Experiment

The sensing experiment was carried out using different anions viz., MnO_4^-, $HAsO_4^{2-}$, AsO_3^{3-}, Cl^-, $Cr_2O_7^{2-}$, F^-, I^-, MoO_4^{2-}, $S_2O_8^{2-}$, SeO_4^{2-}, SeO_3^{2-}, SO_4^{2-}, SO_3^{2-} and $S_2O_3^{2-}$. 5 mg of the solid nano particle was taken in 0.5 mL of water and then sonicated for 30 mins. This solution was called as the nanoparticle solution. Then 20 µL of this solution was taken in 2 mL of water in a cuvette. Finally, this solution was treated with different aliquots of 0.1 mM of different analytes. The results were analyzed using UV-Vis spectroscopy.

3.7. Isothermal Titration Calorimetric (ITC) Analysis

Isothermal Titration Calorimetry (ITC) provided information on the thermodynamic parameters arising out of the interaction of MnO_4^- with Ni-SA NPs. 300 µL of the NP solution was taken in the sample cell. 5 mM $KMnO_4$ was taken in the syringe and 2 µL aliquots were gradually added into the cell. During the experiment, deionized water was used as blank. The calorimetric titrations were carried out for 50 mins at 25º C. The molecular interaction between $KMnO_4$ and NPs can be defined by the following thermodynamic equation (Eq. 1) based on an ITC analysis:

$$\Delta G = \Delta H - T\Delta S \qquad (1)$$

Where ΔG is the change in Gibbs free energy, ΔH is enthalpy change, ΔS is entropy change, and T is the absolute temperature. The binding stoichiometry can also be measured using the ITC experiment.

The value of ΔG can alternatively be calculated using the following equation with the value of the association constant (K_a) (Eq. 2)

$$\Delta G = -RTlnK_a \qquad (2)$$

The universal gas constant, R, is used in this equation.

3.8. Interference Study

The interference study was carried out using different co-existing ions viz. $HAsO_4^{2-}$, AsO_3^{3-}, CrO_4^{2-}, $Cr_2O_7^{2-}$, ClO_4^-, PO_4^{3-}, SeO_4^{2-}, SeO_3^{2-}, K^+, Mn^{2+}, Cr^{3+} and Fe^{3+} of equimolar concentration (0.003 mM) to that of the permanganate anion. 40 µL of the nano particle solution was taken in 2 mL of water. 60 µL of each of the interfering ions (0.1 mM) were added separately to this solution and then treated with 60 µL of $KMnO_4$ solution (0.1 mM). The sensing ability of the nano particle towards the permanganate ion was then analysed using UV-Vis spectrophotometer.

3.9. Analysis of natural samples

Boring water and tap water samples were collected and used as obtained. Sweet potato weighing ~70 g was chopped with a knife and then soaked in 150 mL of distilled water. After 90 min of soaking, the solution was filtered with a Whatmann-42 filter paper. 2 mL of distilled water was treated with 40 µL of nanoparticle solution and then a small aliquot of these sample solutions were individually added and the data were analysed using UV-Vis spectrophotometer. The amount of MnO_4^- ion present in the sample was estimated using a pre-calibrated equation. Recovery percentage was also checked with tap water by addition of small aliquots of the $KMnO_4$ solution of known concentration. The absorbance data were collected at 593 nm and with the help of a suitable calibration plot, the recovery % of $KMnO_4$ was calculated.

4. Result and Discussion

Mixing of equimolar concentrations of $NiSO_4$ and sinapic acid solutions causes the light yellow colour of sinapic acid to change into dark brown. This change in color indicates the synthesis of Ni-sinapic acid (Ni-SA NPs) nanoparticles.

4.1. UV-Vis spectroscopy

The formation of Ni-SA NPs was characterized using UV-Vis spectroscopy shown in Fig. S1. The characteristic absorption peak of SA (355 nm) at pH 11 disappeared upon formation of the nanocomposite and a new peak appeared at 298 nm. This also indicates that the formation of Ni-SA NPs [62, 63, 64].

4.2. FTIR

Due to the interaction between the $NiSO_4$ and sinapic acid, a major shift in the IR frequency was observed as compared to the pure sinapic acid. Fig. 1 shows three relevant regions: region (a) around 3500-2400 cm^{-1}, region (b) around 1800-1000 cm^{-1}, and region (c) around 1000-500 cm^{-1}. Region (a) was developed mainly due to the hydroxyl group and $-CH_3$ group. Region (b) was obtained for C=O stretching frequency of –COOH group, aromatic ring, and C-O-C stretching frequency. Region (c) was formed mainly due to the bending vibrations.

The result showed that the admissible change in the vibrational frequency was observed mainly in region (a) and region (b) suggesting the participation of the –COOH group along with the benzene ring of the sinapic acid towards the complexation with $NiSO_4$. The peak observed at 3383 cm^{-1} and 3311 cm^{-1} in the pure sinapic acid was shifted and developed a higher intense peak at 3425 cm^{-1} in the nano particles. The peaks in the range of 3021 cm^{-1} - 2837 cm^{-1} were also modified due to the formation of nano particles. The conjugated carbonyl peak at 1663 cm^{-1} coming from the –COOH of the pure sinapic acid was diminished upon formation of the nanoparticle. The intensity of the peaks in the range 1594 cm^{-1} – 1433 cm^{-1} was also modified in presence of $NiSO_4$ solution. The peaks due to $–CH_3$ bending and –C-O-C- stretching either disappeared or their intensities diminished due to the interaction between the $NiSO_4$ and sinapic acid. The region (c) was also modified upon nanoparticle formation. Table S2 shows the results of individual bond vibrations with their possible functionalities [65].

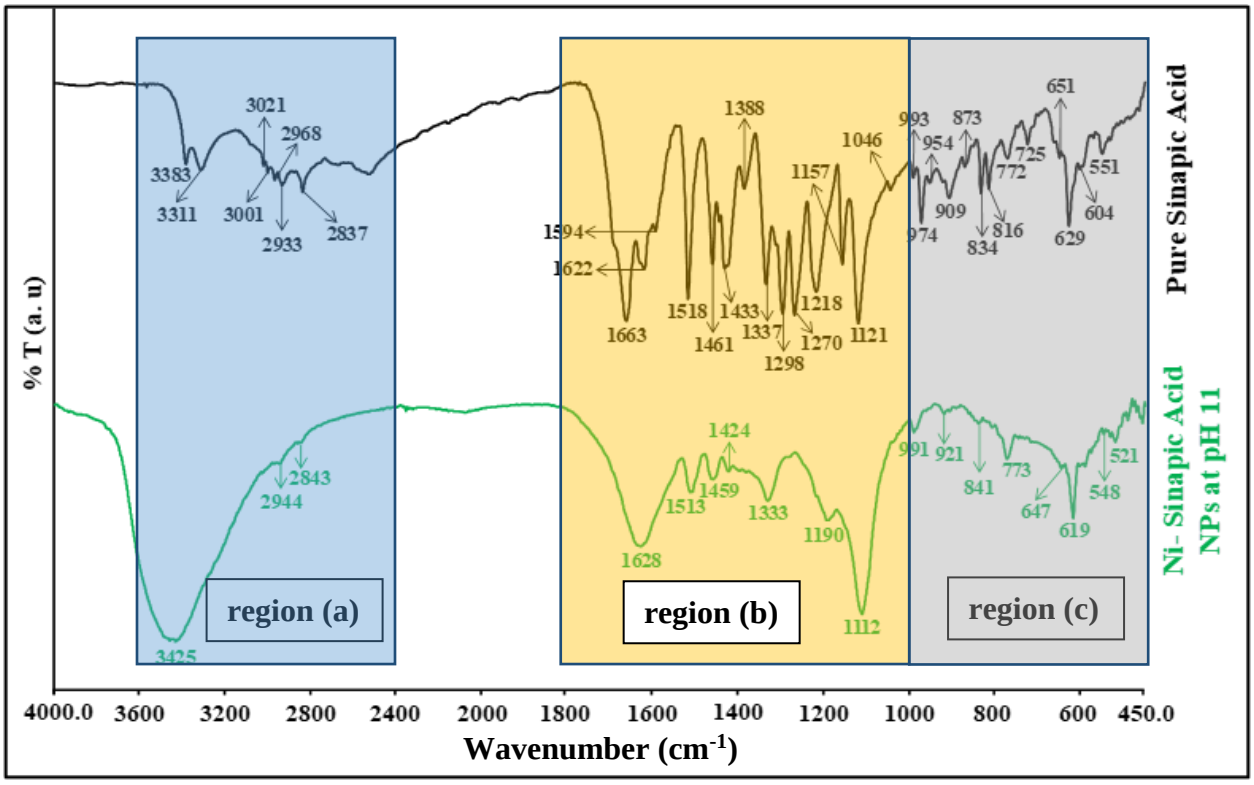

Fig. 1.FTIR spectra of pure sinapic acid and Ni-SA NPs.

4.3. TEM

The nano dimension of the Ni-SA NPs was confirmed from the TEM images of the NPs (Fig. 2a and 2b). The particle size was around 5 to 10 nm with intermittent pores. Clear lattice fringes were observed from a slightly zoomed in TEM image suggesting the nano crystallinity of the NPs (Fig.2b). Fig. 2c shows the histogram for particle size distribution of the NPs with maximum number of particles having 7 nm size. The selected area electron diffraction (SAED) pattern of the NPs showed concentric rings again confirming the nano crystallinity of the NPs (Fig. 2d). The spots arose due to the diffraction from (231), (310), (049), (2210), (703) and (12$\bar{6}$) planes which are shown in the SAED pattern.

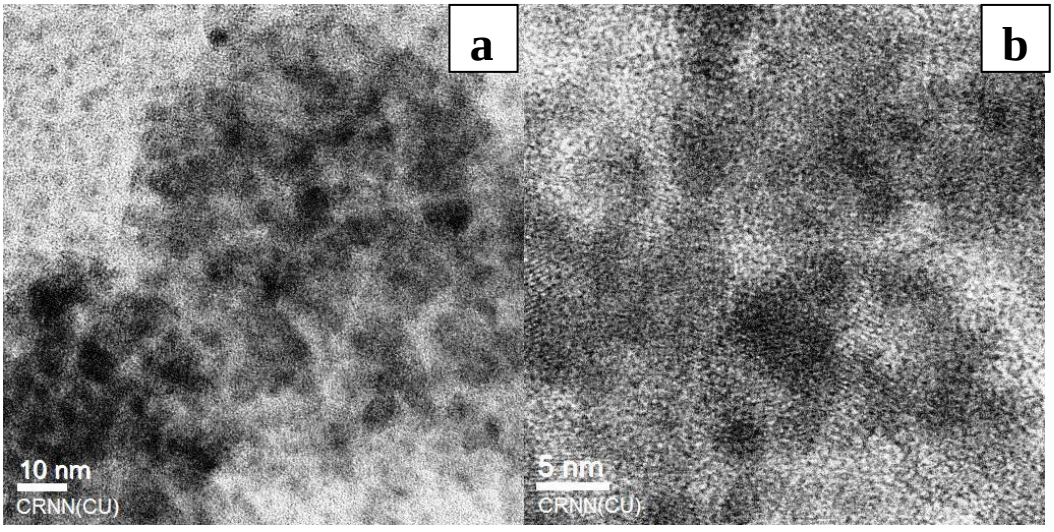

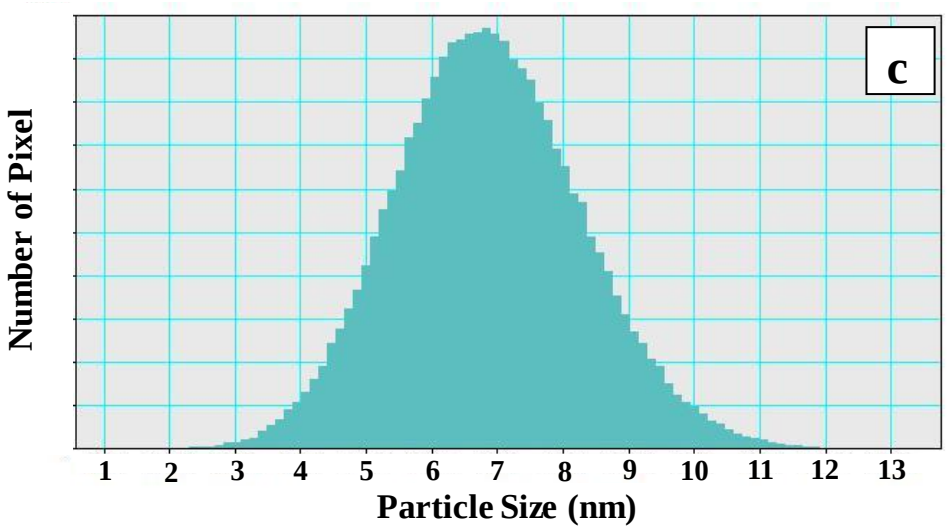

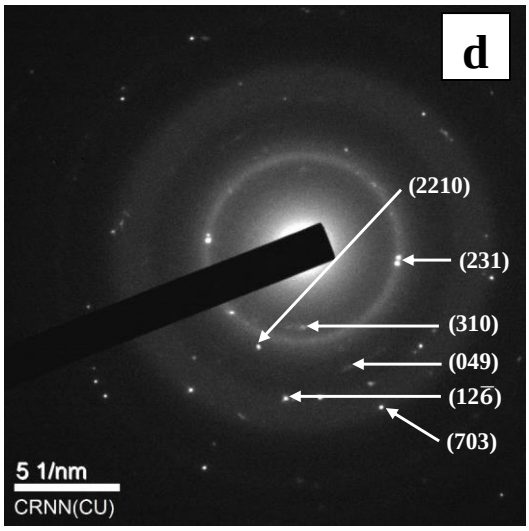

Fig. 2.(a) and (b) represent the TEM images of Ni-SA NPs and (c) histogram showing particle size distribution of Ni-SA NPs (d) SAED pattern of the Ni-SA NPs.

4.4. PXRD

The obtained PXRD (Fig.S2) data were then compared with the unique number from the Joint Committee on Powder Diffraction Standards (JCPDS) (Table S3). For Ni-SA NPs, the major diffractions came from 2θ values 23.024°, 33.886º and 60.164° which correspond to ($\bar{2}$11), (310) and ($\bar{1}$15) and ($\bar{3}$22) planes respectively. The PXRD data suggested that the possible crystallographic systems are monoclinic, tetragonal, anorthic and cubic with majority of them having primitive lattice. The obtained PXRD pattern is similar to the β-phase of $Ni(OH)_2$ [66, 67]. The presence of Ni as $Ni(OH)_2$ was further verified from the XPS data discussed later.

4.5. XPS

XPS analysis of the Ni-SA NPs reveals the presence of C, O, N and Ni, the total concentrations of which are given in the table (Table S4) and confirms the presence of SA with the Ni NPs. The atomic percentage of C, O, N and Ni are 66.30 %, 29.30 %, 0.50 % and 3.90 %respectively.

The binding energy of the $Ni(2p_{3/2})$ peak is found at 856.30 eV, which we attribute to $Ni(OH)_2$. Whilst this value is approximately 1 eV higher than that observed for bulk $Ni(OH)_2$ [68], it is consistent with many examples reported in the NIST XPS database [69]. It is also well established that both electronic and particle size effects can influence the observed binding

energy [70], with nanoparticulate materials often having higher than expected binding energies [71]. Furthermore, the Ni(2p) spectrum (Fig. S3) exhibits a spectral envelope broadly consistent with that of $Ni(OH)_2$ which supports this attribution and the Ni-O frequencies observed in the FTIR analysis. It is likely that NiOOH species are also present based on the spectral envelope, however whilst fitting the data using published models [71] did not yield a satisfactory fit, we do not exclude some small amount being present.

4.6. Sensing

The sensing study was carried out using absorption spectroscopy. There was no spectral change observed for any of the analytes except permanganate ions. Gradual addition of very small aliquots of permanganate ions, results in the formation of a new peak at 603 nm and decrease of characteristic absorption peak of the Ni-SA NPs (298 nm) (Fig. 3).The increase in absorption at 603 nm was observed up to 2 µM concentration of the analyte which symbolizes the interaction between Ni-SA NPs with the permanganate ion and the decrease in the absorption peak at 298 nm was due to dilution of the nano particle solution in presence of minute amount of analyte. The limit of detection is 413 nM and the linear range for this detection is 1.25 to 1.70 µM with correlation coefficient of 0.95. The different analytical parameters for the detection of the $KMnO_4$ ion is tabulated in Table 1.

No spectral change was observed for all the other analytes and the respective UV-Vis spectra are presented in the supplementary file (Fig.S4-S16). The selectivity of the Ni-SA NPs towards the permanganate ion is represented in Fig. S17.

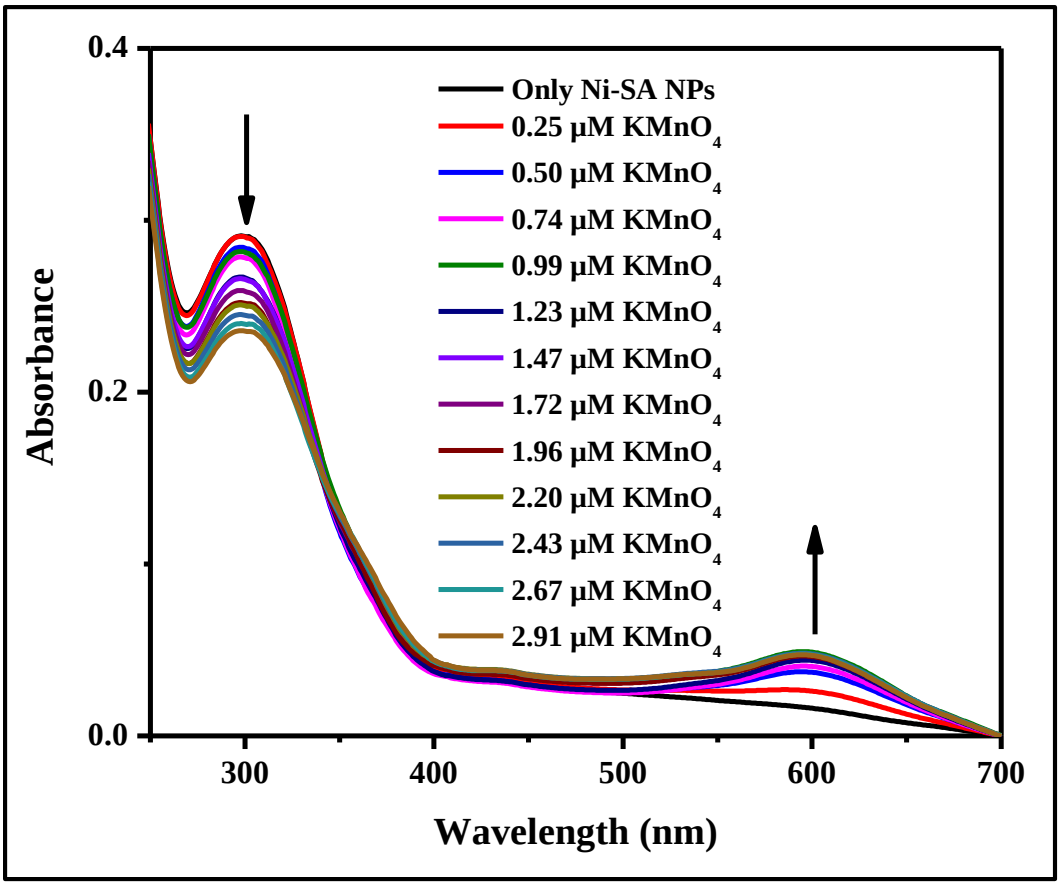

Fig. 3. Spectral change of nano particle solution in presence of permanganate ion (0-3 µM).

Table 1

Different analytical parameters for the detection of the $KMnO_4$.

Parameter	Data
Regression equation	Y = sX+C
Slope (s) (μM^{-1})	0.01
Intercept (C)	0.03
Correlation coefficient (R^2)	0.95
Standard deviation (σ)	0.001
Limit of detection (LOD = 3.3× σ/s) (µM)	0.41
Limit of quantification (LOQ = 10× σ/s) (µM)	1.25
Linear range (µM)	1.25 to 1.70
λ (nm)	603

4.7. Sensing Mechanism

The sensing mechanism was studied using two different techniques viz., ITC and XPS analysis.

4.7.1. ITC

ITC was used to investigate the sensing mechanism and obtain a comprehensive picture of the thermodynamic parameters for the interaction of $KMnO_4$ with the NPs. At 298 K, the interaction between $KMnO_4$ with the NPs was investigated in aqueous medium. The stoichiometry of interaction between $KMnO_4$ with the NPs was found to be 1:1, with an association constant (K_a) of 1.54×10^4 M^{-1} (Fig. 4). The changes in enthalpy (ΔH) and entropy (ΔS) associated with this interaction are -80 kcal/mol and -2.97 kcal/mol/deg, respectively. The ΔG value obtained from the experiment is -5.72 kcal/mol.

Therefore, the interaction process between $KMnO_4$ with the NPs appears to be an enthalpy driven process.

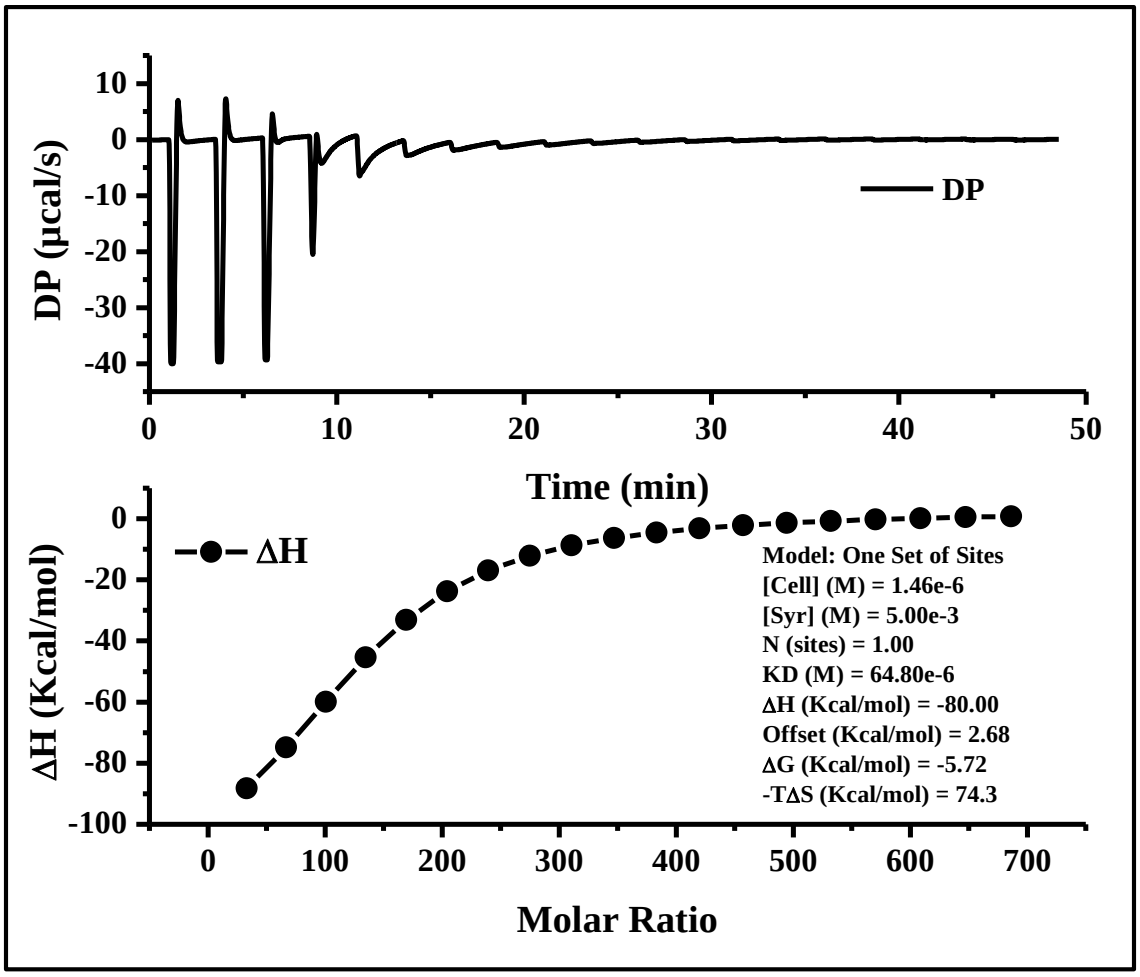

Fig.4. ITC data for binding isotherm for interaction between $KMnO_4$ with the NPs at 298 K.

4.7.2. XPS

Analysis of the permanganate treated sample revealed the presence of K and Mn in addition to the C, O and Ni previously noted for the Ni-SA NPs. The Ni($2p_{3/2}$) binding energy here is found to be 855.4 eV (Fig. 5(a)), almost 1 eV lower than Ni-SA NPs sample. Whilst remaining in the Ni(II) oxidation state, the shift downward in energy is accompanied by a change in the spectral envelope with a somewhat sharper signal in the satellite structure above 860 eV (Fig.5(b)). The binding energy of 855.4 eV is broadly consistent with that of bulk $Ni(OH)_2$ and NiOOH species, with the sharper satellite structure likely indicative of a greater hydroxide content.

Analysis of the Mn($2p_{3/2}$) signal (not shown) is slightly complicated by its superposition on the Ni Auger. Nevertheless, a broad asymmetric peak centred at 642.5 eV is observed. This binding

energy is significantly lower than $KMnO_4$ (645.5 eV), so cannot be ascribed solely to the permanganate, an observation which is confirmed by the relative percentages of K and Mn in the atomic % table (Table S5). The atomic percentage of C, O, Ni, K and Mn are 22.4 %, 47.2 %, 5.4 %, 4.3 % and 20.8 % respectively. Analysis of the spectral envelope shows no sharp peak structure associated with MnO_2, and hence we attribute the Mn speciation to be Mn_2O_3 and/or MnOOH based on the data envelope alone [72].

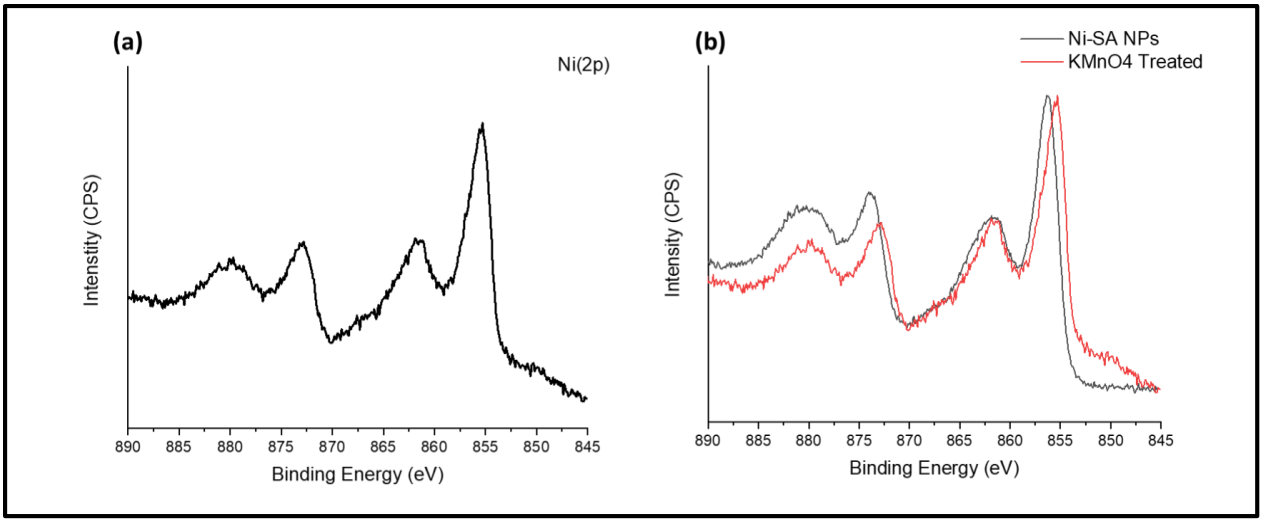

Fig. 5.(a) Ni(2p) core-level spectrum from the $KMnO_4$ treated Ni-SA NPs and (b) normalised overlay of the Ni(2p) spectra from the two materials.

Upon treatment with $KMnO_4$, the organic part containing SA was found to become oxidized by the MnO_4^- ion. The amount of inorganic Ni content increased while the C content was found to decrease. The atomic percentage of O was increased due to the simultaneous oxidation of the organic sphere and the presence of Mn as Mn_2O_3 and/or MnOOH (Table S4 and S5).

Overall, the mechanism can be summarised as an oxidation of the organic sphere attached to the Ni(II) of Ni-SA by the permanganate ions which itself gets reduced from Mn(VII) to Mn(III). Mn remains in the system as Mn_2O_3 and/or MnOOH as has been revealed by XPS. Reduction of Mn(VII) to Mn(III) occurs in neutral medium as can be observed from the experimental findings which also agrees with previous reports [73, 74]. The absorption spectral sensing (Fig.3) shows

appearance of the new peak at 603 nm which gradually increases with increasing permanganate concentration. This appears due to $n \rightarrow \pi^*$ transition of unshared electrons of O present in Mn_2O_3 to one of the antibonding orbitals of the oxidized organic sphere. The intensity of the peak grows with increasing population of 'n' which again is dependent on the concentration of the added analyte (permanganate, which gets reduced to yield Mn_2O_3).

4.8. Interference

The interference experiment was carried out in the presence of other cations and anions at the same concentration as that of MnO_4^- ion. The obtained results (Fig.S18) indicated that there was no significant interference from any of the ions in the detection of trace amounts of MnO_4^- ion. Hence, this process offers a high selectivity for sensing of MnO_4^- ion in the presence of other co-existing cations and anions.

4.9. Analysis of natural samples

Practicability of the present technique has been examined upon analyses of the natural samples. The analyses suggested that, all the studied samples have permanganate contamination and this has been proved using the current methodology. The maximum contamination was obtained for the water sample from Sonarpur area (256.25 μM). The water sample from Garia also contains measurable amount of $KMnO_4$ (94.88 μM). The source of this contamination may have come from the water treatment done using $KMnO_4$ at the reservoir of the water. The colour of the sweet potato in most of the cases is due to the addition of $KMnO_4$ and other contaminants. The extract of sweet potato was in fact found to contain $KMnO_4$ in a measurable amount (~154 μM). The tap water collected from Rajabazar area did not show any measurable amount of $KMnO_4$.

The spectral changes were instantaneous and the spectra remained unaffected with longer incubation times. Each experiment was repeated for three consecutive times and the precision of the results is reflected standard deviation shown in the table. The recovery percentage of $KMnO_4$ from tap water was also examined and the results (Table 2) show that ~88 to 108 % of the added $KMnO_4$ could be recovered. Hence the methodology can be equally applicable towards the environmental samples.

Table 2

Recovery percentage of $KMnO_4$ in tap water.

Added (μM)	Found (μM)	Recovery (%)
0.49	0.43 (± 0.02)	88 (± 4.10)
0.97	1.00 (± 0.05)	103 (± 5.05)
1.44	1.43 (± 0.07)	99 (± 5.00)
2.86	3.00 (± 0.15)	105 (± 5.13)
3.32	3.57 (± 0.18)	107 (± 5.45)
3.77	3.86 (± 0.19)	102 (± 5.40)

5. Conclusion

The Ni-SA NP material is a suitable candidate for a simple cost effective absorption based spectrophotometric sensing of MnO_4^- ions. The method of synthesis of the nanoparticles is also simple and environment friendly as the polyphenolic acid chosen for nano-synthesis is nature derived. Moreover, the methodology is also hazard free. The prepared NPs can sense MnO_4^- ions at micromolar range (μM) and the sensing technique involves no interference from contemporary ions. The enthalpy driven interaction between Ni-SA NPs and the $KMnO_4$ was further studied using XPS analysis. The atomic percentage of different atoms including Ni(II) was varied in presence of the MnO_4^- ion. The organic compound (SA) was found to get affected upon permanganate treatment, which was ascertained from the XPS analysis. However, a short linear dynamic range is a drawback of the present method which may be overcome be judicious sample dilution. Applicability of the present technique has also been studied towards natural water samples and in vegetable. Around 88 to 108% of $KMnO_4$ could be recovered from natural sample. The technique and limit of detection of the present method has been compared (Table S1) with the literature and is found to be at per even after using solvent free conditions and simple instrumentation.

Acknowledgement

PM is thankful to SVMCM for his fellowship. PS expresses sincere thanks to the University Grants Commission (UGC) (Ref. No. of PS 20/12/2015(ii) EU-V dated 24.08.2016) for providing necessary fellowship. AB gratefully acknowledges financial support of WBDST (546(sanc.)/ST/P/S&T/4G-13/2014) and also the FRPDF grant from Presidency University. The

authors are thankful to UGC-DAE-CSR, Kolkata Centre, India, for providing FTIR measurement facility. The authors are thankful to DST FIST (SR/FST/CS-II/2017/27(C) dated 29.09.2018) for the funding of PXRD and ITC instrument.

References

[1] A.A. Ezhilarasi, J.J. Vijaya, K. Kaviyarasu, M. Maaza, A. Ayeshamariam, L.J. Kennedy, P.B. Biology, Green synthesis of NiO nanoparticles using *Moringa oleifera* extract and their biomedical applications: Cytotoxicity effect of nanoparticles against HT-29 cancer cells, J. Photochem. Photobiol. B: Biol., 164 (2016) 352-360. https://doi.org/10.1016/j.jphotobiol.2016.10.003

[2] K. Lokesh, G. Kavitha, E. Manikandan, G.K. Mani, K. Kaviyarasu, J.B.B. Rayappan, R. Ladchumananandasivam, J.S. Aanand, M. Jayachandran, M. Maaza, Effective ammonia detection using n-ZnO/p-NiO heterostructured nanofibers, IEEE Sensors Journal, 16(8) (2016) 2477-2483. 10.1109/JSEN.2016.2517085

[3] F. Fang, J. Kennedy, D. Carder, J. Futter, P. Murmu, A. Markwitz, Nanotechnology, Modulation of field emission properties of ZnO nanorods during arc discharge, J. Nanosci. Nanotechnol., 10(12) (2010) 8239-8243. https://doi.org/10.1166/jnn.2010.3009

[4] F. Fang, J. Futter, A. Markwitz, J. Kennedy, UV and humidity sensing properties of ZnO nanorods prepared by the arc discharge method, Nanotechnology, 20(24) (2009) 245502. http://dx.doi.org/10.1088/0957-4484/20/24/245502

[5] E. Manikandan, J. Kennedy, G. Kavitha, K. Kaviyarasu, M. Maaza, B. Panigrahi, U.K. Mudali, Compounds, Hybrid nanostructured thin-films by PLD for enhanced field emission performance for radiation micro-nano dosimetry applications, J. Alloys Compd., 647 (2015) 141-145. https://doi.org/10.1016/j.jallcom.2015.06.102

[6] C.M. Magdalane, K. Kaviyarasu, J.J. Vijaya, B. Siddhardha, B. Jeyaraj, Photocatalytic activity of binary metal oxide nanocomposites of CeO_2/CdO nanospheres: investigation of optical and antimicrobial activity, J. Photochem. Photobiol. B: Biol., 163 (2016) 77-86. https://doi.org/10.1016/j.jphotobiol.2016.08.013

[7] K. Kaviyarasu, A. Ayeshamariam, E. Manikandan, J. Kennedy, R. Ladchumananandasivam, U.U. Gomes, M. Jayachandran, M.Maaza, Solution processing of CuSe quantum dots:

Photocatalytic activity under RhB for UV and visible-light solar irradiation, Mater. Sci. Eng. B, 210 (2016) 1-9. https://doi.org/10.1016/j.mseb.2016.05.002

[8] K. Kaviyarasu, A. Raja, P.A. Devarajan, Structural elucidation and spectral characterizations of Co_3O_4 nanoflakes,Spectrochim. Acta A: Mol. Biomol. Spectrosc., 114 (2013) 586-591. https://doi.org/10.1016/j.saa.2013.04.126

[9] K. Kaviyarasu, P.A. Devarajan, A versatile route to synthesize MgO nanocrystals by combustion technique, ChemInform, 43(17) (2012) no. DOI: 10.1002/chin.201217219

[10] I. Brigger, C. Dubernet, P. Couvreur, Nanoparticles in cancer therapy and diagnosis, Adv. Drug Deliv. Rev., 64 (2012) 24-36. https://doi.org/10.1016/j.addr.2012.09.006

[11] A.K. Gupta, M. Gupta, Cytotoxicity suppression and cellular uptake enhancement of surface modified magnetic nanoparticles, Biomaterials, 26(13) (2005) 1565-1573. https://doi.org/10.1016/j.biomaterials.2004.05.022

[12] H. Gebretinsae, M. Tsegay, Z.J. Nuru, Biosynthesis of nickel oxide (NiO) nanoparticles from cactus plant extract, Materials Today: Proceedings, 36 (2021) 566-570. https://doi.org/10.1016/j.matpr.2020.05.331

[13] A.A. Ensafi, N. Ahmadi, B. Rezaei, Chemical, Nickel nanoparticles supported on porous silicon flour, application as a non-enzymatic electrochemical glucose sensor, Sens. Actuators B: Chem., 239 (2017) 807-815. https://doi.org/10.1016/j.snb.2016.08.088

[14] J.M. Khurana, S. Yadav, Highly monodispersed PEG-stabilized Ni nanoparticles: proficient catalyst for the synthesis of biologically important spiropyrans, Aust. J. Chem., 65(3) (2012) 314-319. http://sci-hub.tw/10.1071/CH11444

[15] R. Bussamara, D. Eberhardt, A.F. Feil, P. Migowski, H. Wender, D.P. de Moraes, G. Machado, R.M. Papaléo, S.R. Teixeira, J. Dupont, Sputtering deposition of magnetic Ni nanoparticles directly onto an enzyme surface: a novel method to obtain a magnetic biocatalyst, Chem. Comm., 49(13) (2013) 1273-1275. https://doi.org/10.1039/C2CC38737A

[16] K.B. Lee, S. Park, C.A. Mirkin, Multicomponent magnetic nanorods for biomolecular separations, Angew. Chem. Int. Ed., 43(23) (2004) 3048-3050. https://onlinelibrary.wiley.com/journal/15213773

[17] P. Kalita, J. Singh, M. Kumar Singh, P.R. Solanki, G. Sumana, B. D. Malhotra, Ring like self assembled Ni nanoparticles based biosensor for food toxin detection, Appl. Phys. Lett., 100(9) (2012) 093702. https://doi.org/10.1063/1.3690044

[18] P. T. Hernández, M.V. Kuznetsov, I.G. Morozov, I.P. Parkin, Application of levitation-jet synthesized nickel-based nanoparticles for gas sensing, Mater. Sci. Eng. B, 244 (2019) 81-92. https://doi.org/10.1016/j.mseb.2019.05.003

[19] K. Ravindhranath, M. Ramamoorty, Nickel based nano particles as adsorbents in water purification methods-a review, Orient. J. Chem., 33(4) (2017) 1603. http://dx.doi.org/10.13005/ojc/330403

[20] C.J. Pandian, R. Palanivel, S. Dhananasekaran, Green synthesis of nickel nanoparticles using Ocimum sanctum and their application in dye and pollutant adsorption, Chin. J. Chem. Eng., 23(8) (2015) 1307-1315. https://doi.org/10.1016/j.cjche.2015.05.012

[21] W. Sun, L. Xiao, X. Wu, Compounds, Facile synthesis of NiO nanocubes for photocatalysts and supercapacitor electrodes, J. Alloys Compd., 772 (2019) 465-471. https://doi.org/10.1016/j.jallcom.2018.09.185

[22] M. Qamar, M. Gondal, Z.H.Yamani, Synthesis of nanostructured NiO and its application in laser-induced photocatalytic reduction of Cr (VI) from water, J. Mol. Catal. A: Chem., 341(1-2) (2011) 83-88. https://doi.org/10.1016/j.molcata.2011.03.029

[23] C. Jeyaraj Pandian, R. Palanivel, S. Dhanasekaran, Screening antimicrobial activity of nickel nanoparticles synthesized using Ocimum sanctum leaf extract, J. Nanomater., 2016 (2016). http://dx.doi.org/10.1155/2016/4694367

[24] A.A. Ezhilarasi, J.J. Vijaya, K. Kaviyarasu, X. Zhang, L.J. Kennedy, Interfaces, Green synthesis of nickel oxide nanoparticles using *Solanum trilobatum* extract for cytotoxicity, antibacterial and photocatalytic studies, Surf. Interfaces, 20 (2020) 100553. https://doi.org/10.1016/j.surfin.2020.100553

[25] C.J. Pandian, R. Palanivel, U. Balasundaram, Green synthesized nickel nanoparticles for targeted detection and killing of S. typhimurium, J. Photochem. Photobiol. B: Biol., 174 (2017) 58-69. https://doi.org/10.1016/j.jphotobiol.2017.07.014

[26] C.T. Petit, M.S. Alsulaiman, R. Lan, S.. Tao, Direct Synthesis of Ni Nanoparticles by a Non-Aqueous Sol–Gel Process, Nanosci. Nanotechnol. Lett., 4(2) (2012) 136-141. https://doi.org/10.1166/nnl.2012.1302

[27] Y.I. Golovin, D.Y. Golovin, A. Shuklinov, R. Stolyarov, V.M. Vasyukov, Electrodeposition of nickel nanoparticles onto multiwalled carbon nanotubes, Tech. Phys. Lett., 37(3) (2011) 253-255. http://sci-hub.tw/10.1134/S1063785011030217

[28] H. Wang, X. Jiao, D. Chen, Monodispersed nickel nanoparticles with tunable phase and size: synthesis, characterization, and magnetic properties, J. Phys. Chem. C, 112(48) (2008) 18793-18797. https://doi.org/10.1021/jp805591y

[29] E. Ramírez-Meneses, A.M. Torres-Huerta, M.A. Dominguez-Crespo, M. Ponce-Varela, M. Hernández-Pérez, I. Betancourt, E. Palacios-González, Synthesis and electrochemical characterization of Ni nanoparticles by hydrazine reduction using hydroxyethyl cellulose as capping agent, Electrochim. Acta, 127 (2014) 228-238. https://doi.org/10.1016/j.electacta.2014.02.004

[30] Z. Sabouri, A. Akbari, H.A. Hosseini, M. Darroudi, Facile green synthesis of NiO nanoparticles and investigation of dye degradation and cytotoxicity effects, J. Mol. Struct., 1173 (2018) 931-936.https://doi.org/10.1016/j.molstruc.2018.07.063

[31] E.R. Beach, K. Shqau, S.E. Brown, S.J. Rozeveld, P.A. Morris, Physics, Solvothermal synthesis of crystalline nickel oxide nanoparticles, Mater. Chem. Phys., 115(1) (2009) 371-377. https://doi.org/10.1016/j.matchemphys.2008.12.018

[32] B. Anandan, V. Rajendran, Morphological and size effects of NiO nanoparticles via solvothermal process and their optical properties, Mater. Sci. Semicond. Process., 14(1) (2011) 43-47. https://doi.org/10.1016/j.mssp.2011.01.001

[33] G. Madhumitha, G. Elango, S.M. Roopan, biotechnology, Biotechnological aspects of ZnO nanoparticles: overview on synthesis and its applications, Appl. Microbiol. Biotechnol.,100(2) (2016) 571-581. http://sci-hub.tw/10.1007/s00253-015-7108-x

[34] M. Mohammadijoo, Z.N. Khorshidi, S. Sadrnezhaad, V. Mazinani, Synthesis and characterization of nickel oxide nanoparticle with wide band gap energy prepared via thermochemical processing, Nanosci. Nanotechnol. Int. J, 4(1) (2014) 6-9.

[35] P. Karpagavinayagam, A.E.P. Prasanna, C. Vedhi, Eco-friendly synthesis of nickel oxide nanoparticles using Avicennia Marina leaf extract: Morphological characterization and electrochemical application, Mater. Today: Proceedings, (2020). https://doi.org/10.1016/j.matpr.2020.04.183

[36] Z. Sabouri, A. Akbari, H.A. Hosseini, M. Khatami, M.Darroudi, Egg white-mediated green synthesis of NiO nanoparticles and study of their cytotoxicity and photocatalytic activity, Polyhedron, 178 (2020) 114351. https://doi.org/10.1016/j.poly.2020.114351

[37] S.S. Mati, S.S. Roy, S. Chall, S. Bhattacharya, S.C. Bhattacharya, Unveiling the groove binding mechanism of a biocompatible naphthalimide-based organoselenocyanate with calf thymus DNA: an “ex vivo” fluorescence imaging application appended by biophysical experiments and molecular docking simulations, J. Phys. Chem. B, 117(47) (2013) 14655-14665. https://doi.org/10.1021/jp4090553

[38] B.K. Paul, N. Guchhait, Exploring the strength, mode, dynamics, and kinetics of binding interaction of a cationic biological photosensitizer with DNA: implication on dissociation of the drug–DNA complex via detergent sequestration, J. Phys. Chem. B, 115, no.115(41) (2011) 11938-11949. https://doi.org/10.1021/jp206589e

[39] Y. Ma, G. Zhang, J. Pan, Spectroscopic studies of DNA interactions with food colorant indigo carmine with the use of ethidium bromide as a fluorescence probe, J. Agric. Food Chem., 60(43) (2012) 10867-10875. https://doi.org/10.1021/jf303698k

[40] P. Sengupta, A. Ganguly, A. Bose, A phenolic acid based colourimetric ‘naked-eye’chemosensor for the rapid detection of Cu (II) ions, Spectrochim. Acta A: Mol. Biomol. Spectrosc., 198 (2018) 204-211. https://doi.org/10.1016/j.saa.2018.03.005

[41] P. Sathishkumar, F.L. Gu, Q. Zhan, T. Palvannan, A.R.M. Yusoff, Flavonoids mediated ‘Green’nanomaterials: A novel nanomedicine system to treat various diseases–Current trends and future perspective, Mater.Lett., 210 (2018) 26-30. https://doi.org/10.1016/j.matlet.2017.08.078

[42] J.J. Montomery, Water treatment: principles and design, Principles and design. John Wiley & Sons (1985).

[43] N. Irawati, N.A.M. Yusuf, H.A. Rahman, M. Yasin, H. Ahmad, S.W. Harun, Potassium permanganate (KMnO 4) sensing based on microfiber sensors, Appl. Opt., 56(2) (2017) 224-228. https://doi.org/10.1364/AO.56.000224

[44] L. Na, F. Maohong, J. Van Leeuwen, B. Saha, Y. Hongqun, C.P. Huang, Oxidation of As (III) by potassium permanganate, J. Environ. Sci., 19(7) (2007) 783-786. https://doi.org/10.1016/S1001-0742(07)60131-4

[45] R. Liu, L. Sun, R. Ju, H. Liu, J. Gu, G. Li, Treatment of low-turbidity source water by permanganate pre-oxidation: In situ formed hydrous manganese dioxide as filter aid, Sep. Purif. Technol., 117 (2013) 69-74. https://doi.org/10.1016/j.seppur.2013.04.007

[46] W. Chu, D. Yao, N. Gao, T. Bond, M.R. Templeton, The enhanced removal of carbonaceous and nitrogenous disinfection by-product precursors using integrated permanganate oxidation and powdered activated carbon adsorption pretreatment, Chemosphere, 141 (2015) 1-6. https://doi.org/10.1016/j.chemosphere.2015.05.087

[47] Z. Yan, B. Liu, F. Qu, A. Ding, H. Liang, Y. Zhao, G. Li, Control of ultrafiltration membrane fouling caused by algal extracellular organic matter (EOM) using enhanced Al coagulation with permanganate, Sep. Purif. Technol., 172 (2017) 51-58. https://doi.org/10.1016/j.seppur.2016.07.054

[48] F. Faridbod, M.R. Ganjali, M. Hosseini, P. Norouzi, Permanganate selective nano-composite electrode, Int. J. Electrochem. Sci., 7 (2012) 1927-36.

[49] W.A. Welch, Potassium permanganate in water treatment, J. Am. Water Works Assoc., 55(6) (1963) 735-741. https://doi.org/10.1002/j.1551-8833.1963.tb01082.x

[50] J.-X. Wu, B. Yan, Eu (III)-functionalized In-MOF (In (OH) bpydc) as fluorescent probe for highly selectively sensing organic small molecules and anions especially for CHCl3 and MnO4−,J. Colloid Interface Sci., 504 (2017) 197-205. https://doi.org/10.1016/j.jcis.2017.05.054

[51] S.H. Subramanya, V. Pai, I. Bairy, N. Nayak, S. Gokhale, B. Sathian, Potassium permanganate cleansing is an effective sanitary method for the reduction of bacterial bioload on raw Coriandrum sativum, BMC Res. Notes, 11(1) (2018) 1-5. http://sci-hub.tw/10.1186/s13104-018-3233-9

[52] V.A. Lemos, C. G. Novaes, M.A. Bezerra, An automated preconcentration system for the determination of manganese in food samples. J. Food Compos. Anal., 22(4) (2009)337-342. https://doi.org/10.1016/j.jfca.2008.11.019

[53] Y. Tu, Y. Tian, Y.L. Yang, High-sensitivity and selectivity detection of permanganate ions based on pig liver-based carbon quantum dots, Appl. Ecol. Environ. Res., 17(4) (2019) 7249-7263. http://www.aloki.hu/pdf/1704_72497263...

[54] T.-W. Lin, S.-D. Huang, Direct and simultaneous determination of copper, chromium, aluminum, and manganese in urine with a multielement graphite furnace atomic absorption spectrometer, Anal. Chem., 73(17) (2001) 4319-4325. https://doi.org/10.1021/ac010319h

[55] K.C. Teo, J. Chen, Determination of manganese in water samples by flame atomic absorption spectrometry after cloud point extraction, Analyst, 126(4) (2001) 534-537. https://doi.org/10.1039/B008717N

[56] H. Liu, J. Rong, G. Shen, Y. Song, W. Gu, X. Liu, A fluorescent probe for sequential sensing of MnO 4− and Cr 2 O 7 2− ions in aqueous medium based on a UCNS/TMB nanosystem, Dalton Trans., 48(13) (2019) 4168-4175. https://doi.org/10.1039/C9DT00360F

[57] Z. Ye, R. Weng, Y. Ma, F. Wang, H. Liu, L. Wei, L. Xiao, Label-free, single-particle, colorimetric detection of permanganate by GNPs@ Ag core–shell nanoparticles with dark-field optical microscopy, Anal. Chem., 90(21) (2018) 13044-13050. https://doi.org/10.1021/acs.analchem.8b04024

[58] S.Bhattacharyya, D. Rana, S.N. Bhattacharyya, Determination of heat of formation of associated systems by calorimetry, J. Indian Chem. Soc., 74(2) (1997) 103-107. **DOI -: 10.5281/zenodo.5875144**

[59] S.Bhattacharyya, D. Rana, S.N. Bhattacharyya, A thermodynamic study of molecular association by gas liquid chromatography, J. Indian Chem. Soc., 74(6) (1997) 456-463. **DOI -: 10.5281/zenodo.5880620**

[60] S. Bhatiacharyya, D. Rana, S. N. Bhattacharyya, A Thermodynamic Study of Molecular Association by Gas-Liquid Chfomatography : Trilaurylaminealcohol Systems, J. Indian Chem. Soc., 74(7) (1997) 548-551. **DOI -: 10.5281/zenodo.5901630**

[61] N. Fairley, V. Fernandez, M. Richard- Plouet, C. Guillot-Deudon, J. Walton, E. Smith, D. Flahaut, M. Greiner, M. Biesinger, S. Tougaard, D. Morgan, Systematic and collaborative approach to problem solving using X-ray photoelectron spectroscopy, Appl. Surf. Sci. Adv., 5 (2021) 100112. https://doi.org/10.1016/j.apsadv.2021.100112

[62]S. Chandra, A. Kumar, P.K. Tomar, Synthesis of Ni nanoparticles and their characterizations,J. Saudi Chem. Soc., 18 (2014) 437-442.https://doi.org/10.1016/j.jscs.2011.09.008

[63] M. Hemalatha, N. Suryanarayanan, S. Prabahar, Syntehsis and characterization of nickel nanoparticles by chemical reduction method, Optoelectron. Adv. Mater. Rapid Commun., 8 (2014) 288-291.

[64] M. Halder, M. M. Islam, P. Singh, A. Singha Roy, S. M. Islam, K. Sen, Sustainable generation of Ni $(OH)_2$ nanoparticles for the green synthesis of 5-substituted 1 H-tetrazoles: a competent turn on fluorescence sensing of H2O2, ACS omega, 3 (2018) 8169-8180. DOI: 10.1021/acsomega.8b01081

[65] N. K. Fuloria, S. Fuloria, Spectroscopy: Fundamentals and Data Interpretation, Stadium Press India Pvt. Ltd., 2013, ISBN-10: 9380012586

[66] D. S. Hall, D. J. Lockwood, C. Bock, B. R. MacDougall, Nickel hydroxides and related materials: a review of their structures, synthesis and properties. Proc. Roy. Soc. A: Math., Phy. Eng. Sci., 471 (2015) 20140792. https://doi.org/10.1098/rspa.2014.0792

[67] M. El-Kemary, N. Nagy, I. El-Mehasseb, Nickel oxide nanoparticles: synthesis and spectral studies of interactions with glucose. Mater. Sci. Semicond. Process, 16 (2013) 1747-1752. https://doi.org/10.1016/j.mssp.2013.05.018

[68] M.C. Biesinger, B.P. Payne, L.W.M. Lau, A. Gerson, R. C. Smart, X-ray photoelectron spectroscopic chemical state quantification of mixed nickel metal, oxide and hydroxide systems, Surface and Interface Analysis: An International Journal devoted to the development and application of techniques for the analysis of surfaces, interfaces and thin films, 41(4) (2009) 324-332. https://analyticalsciencejournals.onlinelibrary.wiley.com/journal/10969918

[69] A.V. Naumkin, A. Kraut-Vass, S.W. Gaarenstroom, C.J. Powell, NIST X-ray photoelectron spectroscopy database, version 4.1, National Institute of Standards and Technology: Gaithersburg, (2012).

[70] P. Ascarelli, M. Cini, G. Missoni, N. Nistico, XPS line broadening in small metal particles, Le Journal de Physique Colloques, 38(C2) (1977) C2-125-C2-128. https://doi.org/10.1051/jphyscol:1977225

[71] J. Tao, J. Pan, C. Huan, Z. Zhang, J. Chai, S.J. Wang, Origin of XPS binding energy shifts in Ni clusters and atoms on rutile TiO2 surfaces, Surf. Sci., 602(16) (2008) 2769-2773. https://doi.org/10.1016/j.susc.2008.06.034

[72] M.C. Biesinger, B.P. Payne, A.P. Grosvenor, L.W. Lau, A.R. Gerson, R.S.C. Smart, Resolving surface chemical states in XPS analysis of first row transition metals, oxides and hydroxides: Cr, Mn, Fe, Co and Ni, Appl. Surf. Sci., 257(7) (2011) 2717-2730. https://doi.org/10.1016/j.apsusc.2010.10.051

[73] Y. Gao, J. Jiang, Y. Zhou, S.Y. Pang, J. Ma, C. Jiang, Z. Wang, P.X. Wang, L.H. Wang, J. Li, Unrecognized role of bisulfite as Mn (III) stabilizing agent in activating permanganate (Mn (VII)) for enhanced degradation of organic contaminants, Chem. Eng. J., 327 (2017) 418-422. http://dx.doi.org/10.1016/j.cej.2017.06.056

[74] K.A.M. Ahmed, Exploitation of KMnO4 material as precursors for the fabrication of manganese oxide nanomaterials, J. Taibah Univ. for Sci., 10(3) (2016) 412-429. http://dx.doi.org/10.1016/j.jtusci.2015.06.005

Conflict of Interest:

Authors declare no conflict of interest.

Authorship contribution statement

Prasenjit Mondal: Methodology, Investigation, Data curation, Writing (original draft, review, editing);

Pritam Singh: Methodology, Investigation, Data curation;

David Morgan: Investigation, Data curation;

Adity Bose: Supervision, Writing (review);

Kamalika Sen: Conceptualization, Supervision, Writing (review, editing)